Climate Dynamics
https://doi.org/10.1007/s00382-019-04740-1

The Pacific Meridional Mode over the last millennium

Sara C. Sanchez[1] · Dillon J. Amaya[2] · Arthur J. Miller[2] · Shang-Ping Xie[2] · Christopher D. Charles[2]

Received: 25 September 2018 / Accepted: 11 March 2019

Abstract
The Pacific Meridional Mode, a coupled ocean–atmospheric interaction responsible for propagating subtropical anomalies to the tropics via thermodynamic mechanisms, features prominently in discussions of the response of climate variability to climate change. However, it is presently unclear how and why the variance in PMM might change, or even if greenhouse gas forcing might lead to heightened activity. Here, PMM variance over the last millennium is assessed in the Community Earth System Model Last Millennium Ensemble (LME). The model reproduces the main spatial characteristics of the PMM in the modern ocean in agreement with observations. With this basis, we assess the magnitude of the PMM variance over the past millennium, subject to forcing from a variety of sources. Internal (unforced) variability dominates the PMM variance in the LME, but prolonged periods of strong or weak PMM variance are found to be associated with characteristic spatial patterns, consistent across ensemble members and forcing experiments. The pattern of strong PMM variance features a cooler north Pacific, weaker Walker circulation, and a southward-shifted ITCZ. Comparison with a slab ocean model suggests that equatorial ocean dynamics are necessary to sustain the statistically significant multidecadal variability. With respect to the last millennium, present greenhouse forcing does not promote exceptional PMM variance. However, the PMM variability projected in the RCP8.5 scenario exceeds the thresholds expressed with the forcings applied over the Last Millennium. Aside from multidecadal variability, the model simulations also bear on ENSO variability and the sensitivity of climate variability to external forcing.

Keywords Pacific Meridional Mode (PMM) · Decadal climate variability · Paleoclimate · ENSO · Last millennium

1 Introduction

The Pacific Meridional Mode (PMM) is a form of tropical ocean–atmospheric interaction, independent of ENSO, that can create coherent anomalies through an interplay of wind speed and surface evaporation. This mode has been increasingly recognized as an influential component of climate variability, effective in channeling extratropical anomalies to the equatorial ocean–atmosphere system (Chiang and Vimont 2004). The PMM is reinforced by a thermodynamic feedback involving varying wind speed, evaporation, and sea surface temperatures (WES feedback; Xie and Philander 1994; Chang et al. 1997). Central to this mode, extratropical atmospheric variability acts to warm (cool) local sea surface temperatures in the subtropical North Pacific, adjusting the mean surface wind field and spurring lesser (greater) evaporative cooling. These positive (negative) sea surface temperature anomalies, typically initiated southwest of Baja California in the Eastern Tropical North Pacific, induce further weakening (strengthening) of the trade winds by relaxing the meridional surface temperature gradient. These weakened trade winds further reduce (increase) evaporation rates, allowing the sea surface temperature anomalies to propagate southwestward to the equatorial Pacific. The "meridional mode" framework is important as it links El Niño Southern Oscillation (ENSO) variability to internal extratropical atmospheric variability.

Indeed, the PMM was initially hypothesized as an important precursor to ENSO (Chiang and Vimont 2004). This hypothesized connection has been supported in subsequent

Electronic supplementary material The online version of this article (https://doi.org/10.1007/s00382-019-04740-1) contains supplementary material, which is available to authorized users.

✉ Sara C. Sanchez
sasanch@uw.edu

[1] Joint Institute for the Study of the Atmosphere and Ocean, University of Washington, Seattle, WA 98195, USA

[2] Scripps Institution of Oceanography, University of California-San Diego, La Jolla, CA 92037, USA

Published online: 10 April 2019

observational and modelling studies. For example, using instrumental observations between 1958 and 2000, Chang et al. (2007) found that more than 70% of El Niños followed a positive PMM event. This strong relationship has similarly been observed in National Center for Atmospheric Research Community Climate System Model, version 3 (CCSM3, Zhang et al. 2009), and in version 4(CCSM4; Larson and Kirtman 2013), and other CMIP5 models (Lin et al. 2015). The PMM also seems to be important for the formation of central Pacific El Niño (Vimont et al. 2005; Di Lorenzo et al. 2010; Yu et al. 2010; Yu and Kim 2011; Kim and Yu 2012), and, accordingly, the increase in prevalence of the Central Pacific El Niño events over the past few decades has been attributed to an intensification of the thermodynamic coupling mechanism central to the PMM (Di Lorenzo et al. 2015, 2016). The PMM has further been identified as an important feature in Pacific cyclone suppression/enhancement (Zhang et al. 2016), is thought to have played a role in the extreme drought, and sea surface temperatures, and resilience of a mid-level atmospheric high pressure system of 2012–2016 (Wang et al. 2014; Hartmann 2015), the associated marine heat wave (Di Lorenzo and Mantua 2016; Joh and Di Lorenzo 2017), and is an important means of attenuating low frequency variability in the tropics (Di Lorenzo et al. 2015).

While the PMM has proven to be an important feature in the climate system, the recent amplification of PMM variability (Fig. 1c), deserves careful consideration. It is still unknown if and why the variance of the PMM might be intensifying. The apparent increase in variance might simply be the result of unforced modulations in the climate system. Alternatively, this intensification may have been induced by a changing mean state associated with anthropogenic global warming. The background state could influence the PMM through a number of processes: (1) The effectiveness of WES feedback could fluctuate via changes in the mean surface temperature and wind fields (Di Lorenzo et al. 2015; Di Lorenzo and Mantua 2016; Vimont et al. 2009; Liguori and Di Lorenzo 2018), (2) the characteristics of stochastic wind forcing in the extratropics can be modified due to variations in atmospheric circulation (Chiang et al. 2009), and (3) The structure and location of the Intertropical Convergence Zone (ITCZ) could change, potentially allowing for greater propagation of anomalies from the subtropics to the tropics (Zhang et al. 2014a, b; Martinez-Villalobos and Vimont 2016). Instrumental records are simply not long enough to capture the full range of variability of the PMM and to test these alternatives.

Over the last millennium, Earth's radiative budget has fluctuated as a result of a variety of natural and anthropogenic forcings: volcanic eruptions, solar cycles, orbital variation, land use change, greenhouse gas and aerosol emissions. These shifts provide a means of investigating how sensitive the PMM is to subtle variations in the mean state and provide greater context to understand the extent the of natural variability. Therefore, the last millennium represents a valuable experimental platform. Paleoclimatic proxy records (e.g. from corals) provide some indication of PMM variance (e.g. Sanchez et al. 2016), but, are too geographically sparse to pinpoint mechanisms of PMM variability beyond the instrumental record. Thus, temporally extended model integrations are required to make use of the experimental platform.

Here we use the Community Earth System Model-Last Millennium Ensemble (CESM-LME) to better understand the extent of PMM variability, seeking to address the questions of how the modeled PMM changed over the last millennium, and whether the changes were the result of

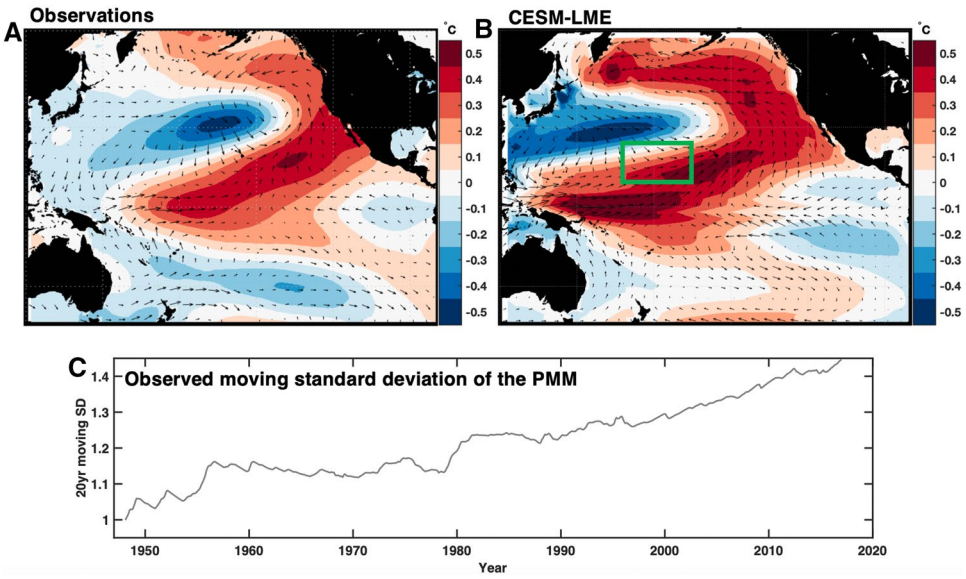

Fig. 1 Linear regression maps between PMM and SST and surface wind vector anomalies **a** in observations, using years 1948–2006 from NOAA ERSSTv3b (Smith et al. 2008) and NCEP–NCAR Reanalysis version 1 (Kalnay et al. 1996) winds and **b** a single ensemble member the CESM-LME using years 1948–2006. The green box outlined highlights the region of NPO DJF zonal wind forcing used in Fig. 6. **c** The moving 20-year standard deviation (using a centered window) of the Pacific Meridional Mode index in observations (relative to the 1948–1968 mean), highlighting the often discussed trend for increasing variance

radiative forcing. The analysis includes the issues of whether the PMM always operated in a physical framework similar to that of the modern climate. We further explore the links between the variability of the PMM and ENSO.

2 Datasets and methodology

The Last Millennium Ensemble (CESM-LME, Otto-Bliesner et al. 2016) and the Large Ensemble (CESM-LE; Kay et al. 2015) experiments use the same coupled physical model of ocean, atmosphere (the Community Atmosphere Model version 5), land, and sea ice. However, the experiments differ in grid cell resolution and forcing employed: the CESM-LME has a coarser land and atmosphere resolution (~ 2° atmosphere and land, ~ 0.3°–1° ocean and sea ice coupled model), while the CESM-LE has a 1° atmosphere model. In addition, the experiments consist of a number of realizations to capture a fuller extent of internal variability in the model behavior. The LME is forced with varying solar intensity, volcanic aerosol emissions, greenhouse gas concentrations, land use changes, orbital variations, aerosols and ozone calibrated with values from observations and high resolution paleoclimate reconstructions. Each LME ensemble member spans 1256 years, beginning in year 850 and extending to 2006 (more information available in Otto-Bliesner et al. 2016). The LME is therefore an especially useful platform for forcing-response diagnosis, given that there are multiple ensemble members within each prescribed forcing regime. The twelve "all-forcing" experiments include all relevant radiative forcing (volcanic, greenhouse gases, ozone-aerosols, land use change, solar intensity, and orbital), while the five volcanic forcing-only ensemble members have only been forced with historical volcanic eruptions. The control (unforced) run provides a measure of internal variability within the model. Finally, the future projections are an extension of four of the all-forcing scenario ensemble members (#2, 3, 8, and 9), following the RCP 8.5 forcing pathway. These ensemble members provide the unique opportunity to not only account for the range of natural variability, but also to pinpoint the common and robust characteristics of the modelled Pacific Meridional Mode. We additionally assess two long unforced control runs in the Community Earth System Model Large Ensemble (CESM-LE, Kay et al. 2015) to gauge the role of ocean dynamics in the variability of the PMM. One control run comes from the fully coupled model (CESM-LE), the other control run comes from a slab ocean experiment using the CAM5 model (CESM-LE–SOM). The CESM model, encompassing the CESM-LME and CESM-LE, are demonstrably skillful in capturing broad aspects of climate variability in the tropical Pacific, but can overestimate the amplitude of ENSO variability (Otto-Bliesner et al. 2016; Kay et al. 2015; Vega-Westhoff and Sriver 2017) (Table 1).

3 Results

3.1 Model validation

The PMM is calculated with similar methodology to Chiang and Vimont (2004); monthly means of sea surface temperatures and 1015 mb zonal and meridional winds from 21°S–32°N, 175°–265°E are removed and 3 month moving average is applied before taking the Maximum Covariance Analysis (MCA) of the three variables. As in observations (Smith et al. 2008; Kalnay et al. 1996), the PMM in CESM-LME is the second mode of maximum

Table 1 Characteristics of model experiments

Model	Years	Ensemble members	Applied forcing
CESM-LME control Otto-Bliesner et al. (2016)	850–2006	1	None
CESM-LME volcanic-only Otto-Bliesner et al. (2016)	850–2006	5	Volcanic
CESM-LME all forcing Otto-Bliesner et al. (2016)	850–2006	12	Greenhouse gases, ozone-aerosols, volcanic, land use change, solar intensity, and orbital volcanic, greenhouse gases, ozone-aerosols, land use change, solar intensity, and orbital
CESM-LME RCP8.5 Otto-Bliesner et al.(2016)	2006–2100	4	Greenhouse gases, ozone-aerosols, volcanic, land use change, solar intensity, and orbital volcanic, greenhouse gases, ozone-aerosols, land use change, solar intensity, and orbital
CESM-LE control Kay et al. (2015)	1–1000	1	None
CESM-LE SOM control Kay et al. (2015)	1–900	1	None

covariance between winds and SST after ENSO, and it is characterized by large sea surface temperature and wind anomalies southwest of Baja California, extending southwestwards towards the dateline (Fig. 1). In the Last Millennium Ensemble, the SST and wind anomalies associated with the PMM are comparable to observations; however, with respect to observations, the mean spatial pattern of SST and wind anomalies is shifted westward and into the Western Pacific Warm Pool region as is common in many GCMs (Kug et al. 2010; Ham and Kug 2012; Capotondi et al. 2006). The correlation of the SST and wind expansion coefficients are slightly stronger in the model than in observations (R = 0.86 vs R = 0.70, respectively), implying marginally stronger air–sea coupling in CESM.

The North Pacific Oscillation (NPO), calculated as the 2nd EOF of sea level pressure in the North Pacific, defined as 180°W–110°W, 25°N–62°N (Walker and Bliss 1932; Rogers 1981; Linkin and Nigam 2008), has been shown to force the PMM in boreal winter (Anderson 2003; Vimont et al. 2003, 2014). Approximately 2–3 months before the PMM peaks, wind anomalies associated with the NPO imprint a pattern of SST anomalies (Fig. 2a). The monthly variance of the PMM is then maximized in March–April–May and can initiate ENSO activity [described by the Niño 3 index as in Kug et al. (2010), 5°S–5°N, 170°–110°W] in the following DJF (9 months later Fig. 2b). This series of steps is qualitatively reproduced in CESM-LME, and furthermore, the variance of the PMM (MAM) is highly correlated with the variance of the following Niño 3 (DJF, Fig. 2d), suggesting that the PMM is a highly effective ENSO precursor. While the standard deviation of the Niño 3 region is directly related to the variability of the NPO (Fig. 2c), the highest correlation coefficients are found in the NPO–PMM–ENSO chain. We note that a weaker correlation is found when the Niño 3 leads the PMM by 14–20 months (mean R = − 0.37 vs mean R = 0.48 when the PMM leads the Niño 3 by 9 months) in the LME, not found in observations. In general, the physical consistency of the model with observations allows us to refer to the variability within CESM-LME to investigate both the internal and forced variability of the PMM.

There are two commonly used metrics for describing the strength of the PMM. The first metric is the 30-year moving standard deviation of the SST expansion coefficient of the PMM MCA index in March–April–May [MAM, the months of highest variance, as in Di Lorenzo and Mantua (2016) and Wang et al. (2014)]. The second is the 30-year moving correlation between the wind and SST expansion coefficients from the maximum covariance analysis [used in other MCA analysis to show greater coupling between variables, as in Amaya et al. (2017) and Lin et al. (2015)]. In the instrumental record, both metrics have shown an increase in variability (Fig. 1c) or in the air–sea coupling affiliated with the PMM (not shown) from years 1950 to the present.

A 30-year moving standard deviation of the PMM is calculated in the unforced control run (Fig. 3a) to provide a baseline expectation for the internal variability observed in the model. This baseline fluctuates roughly by a factor of two and experiences a wider range in variability than that of the forced runs. In CESM-LME, the variability in the 30 year moving correlation between the wind and SST expansion coefficients is mostly uniform in time, even in the forced experiments. However, the rare deviations in the correlation coefficient of the expansion coefficients skew highly negatively, implying that the surface SST or winds are temporarily decoupled. This type of deviation is most common immediately following volcanic eruptions in single ensemble members, but is not found in ensemble averages (not shown). For these reasons, we emphasize the description and assessment of PMM strength using the 30-year moving standard deviation.

3.2 Forced and unforced variability

Internal variability in the climate system (defined as in Deser et al. 2012a, b) dominates the variance of the PMM in each individual ensemble member. In any single ensemble member from each particular forcing experiment, the most pronounced form of variability is low frequency variability, also readily observed in the control run (Fig. 3a, thin grey lines in b, c). In each of the forced experiments, the internal variability is comparable to that of the control run and causes the standard deviation of the PMM to vary by about a factor of two. However, when ensemble members from single forcing experiments are averaged together, the high amplitude internal variability vanishes, as internal variability should not be coherent between ensemble members. This provides a means of identifying forced responses as periods when the ensemble averaged PMM index is above a particular threshold, since forced variability would create coherent anomalies of the same sign between ensemble members, regardless of their internal variability.

In Fig. 3, coherent anomalies in the moving standard deviation of the PMM are found in concert with volcanic eruptions, suggesting that the PMM could be influenced by variations in Earth's radiative budget. Volcanic eruptions tend to amplify the variability of the PMM in the ensemble mean, or more specifically, increase the variance of the PMM's SST expansion coefficient. For example, the Samalas event of 1257 (Lavigne et al. 2013; Guillet et al. 2017), the largest volcanic eruption in the last 2500 years (Lavigne et al. 2013), created a short lived, but high amplitude signal, prompting the epoch of highest averaged variance in the last millennium (Fig. 3b, c). Though this event was only manifest for 3 years, the 30-year moving standard deviation

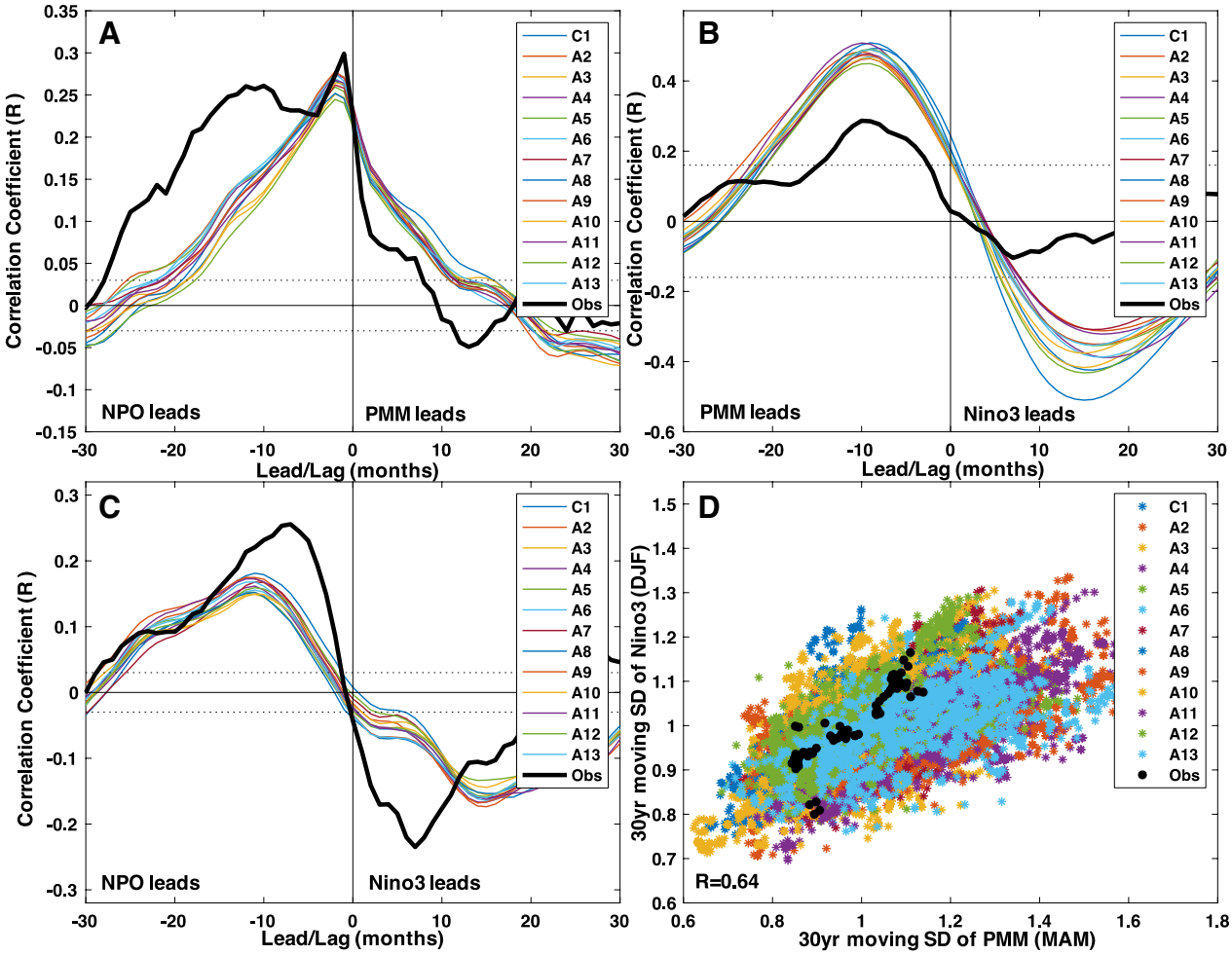

Fig. 2 The model PMM is physically consistent with observations. **a** lead-lag plot in the Control and 12 "All Forcing" experiments (colors) and observations (black) between the PMM and the NPO Index (calculated as the second EOF of SLP in the North Pacific); maximum correlation is found when NPO leads by 2 months), (median maximum correlation, R = 0.27). The dashed lines indicate a $p < 0.01$ significant correlation for the CESM output when accounting for autocorrelation in each index by modifying the number of effective degrees of freedom, as in Bretherton et al. (1999). **b** Same as **a**, but with the PMM and Niño 3 index; a maximum correlation is found when ENSO follows the PMM by 9 months, (median maximum correlation, R = 0.57). Observations here use the wind component of the PMM. **c** For comparison's sake, we also show the cross correlation relationship between the NPO and the Niño 3. As the strength of the correlations are much weaker than that of the NPO-PMM, or PMM-Niño 3, this highlights the important role of the PMM (median maximum correlation, R = 0.17 when the NPO leads by 12 months). **d** Scatterplot of the 30-year moving standard deviation of the PMM (MAM) and the following Niño 3 (DJF)

metric results in the appearance of an artificially prolonged 60-year period of high variance (Supplementary Materials., Figure S1).

Another indication of the PMM's sensitivity to Earth's radiative budget is observed when considering greenhouse gas forcing. In the 12 All-Forcing scenarios, an increase in PMM variance is observed through the late twentieth century (through the year 2006 in the CESM simulations, Fig. 3c). The variance in the "present" is above average, but does not exceed the bounds of that simulated over the last millennium. In a single ensemble member, the variance rises above all previous values, but the average trend suggests that there is no clear difference in the variability of the late twentieth century from the variability witnessed over the last millennium.

3.3 Pattern of variance

Modifications in the background climate have been hypothesized to amplify or dampen the variability of the PMM. The three leading hypotheses describing the ways in which the mean climate might influence the PMM are: (1) The mean location of the ITCZ, (2) the sensitivity of latent heat fluxes to the variations in wind speed are expected to change with the mean background temperature and (3) variations in "noisiness" in the extratropical atmosphere. To investigate

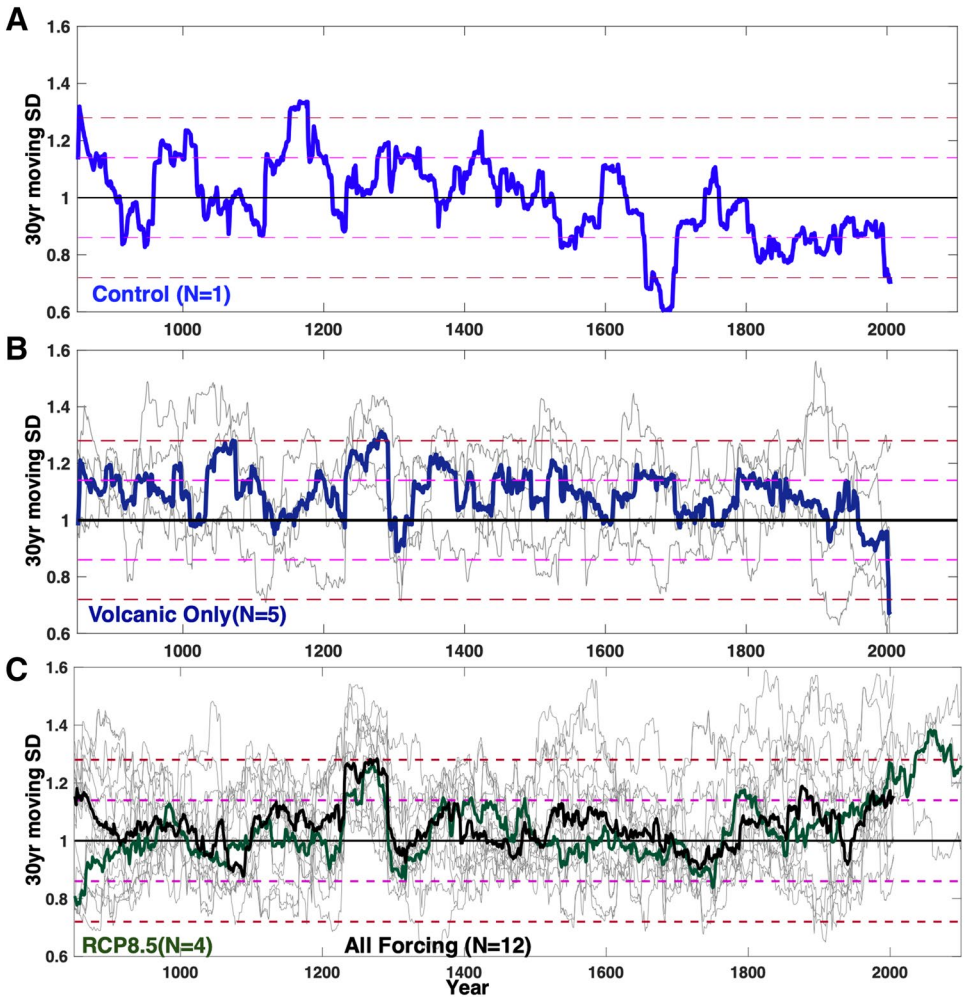

Fig. 3 Moving 30-year standard deviation (centered window) is used on different CESM-LME ensemble members to assess the variability of the PMM over the last millennium. In **a**, the moving 30-year standard deviation of the normalized SST expansion coefficient of the PMM index in the unforced control run. This index is used to estimate a range of PMM variability and the normalization provides a reference for the forced experiments. The 1 sigma mark (±0.14) is dashed in magenta, and the 2 sigma mark is dashed in rust-red. In **b**, the 30-year moving standard deviation of the PMM in each ensemble member from the volcanic-only forcing experiment is plotted in thin gray lines to highlight the range of natural variability within the model. The median of the 5 "Volcanic-Only" experiments is plotted in bolded navy. In **c**, same as **b**, but using the 12 "All Forcing" experiments (median in black) and the four RCP8.5 experiments (median in dark green). The RCP8.5 experiments are a continuation of four of the "All Forcing experiments" (ensemble members #2, 3, 8 and 9) to year 2100

mean state influence on the PMM, we identify the characteristic conditions that accompany periods of extreme PMM variance. There is no reason to expect a clear background pattern of variability, but the existence of a pattern might help address the mechanisms responsible for altering the variance of the PMM.

A least squares linear regression of relevant climate fields is calculated on each of the 30-year moving standard deviation of the PMM (MAM) indices from each of the 12 "All Forcing" ensemble members. A consistent pattern of variability emerges in the averaged ensemble members (Fig. 4). Periods of high variance are characterized by anomalously cool North Pacific sea surface temperatures (of about 0.2 °C for 1 standard deviation) and cooler warm pool region, while the eastern equatorial Pacific and Kuroshio region shows a slight warming tendency. The surface wind field and precipitation response are also consistent with a weaker Walker Circulation during periods of higher variance, while lower PMM variance tends to be characterized by a strengthened Walker Cell and warmer North Pacific. The precipitation response during periods of high PMM variance also features a contracted, southward shifted ITCZ. The same analysis is performed with Pacific mixed layer depth and results in a consistent pattern in the background state associated with PMM variance; high variance is associated with a deepening of the western Pacific and far eastern Pacific mixed layer depth and shoaling of central equatorial mixed layer depth, with shoaled flanks extending eastward in the extratropics (Fig. 4). The PMM variance pattern is a robust feature in CESM, regardless of forcing experiment and method of calculation. Compositing of the most extreme (top quintile) events results in essentially the identical pattern of anomalies in each respective climate fields (see the Supplementary Materials, Figure S2).

There is some consistency between these background patterns associated with the internal variability of the PMM and the previously hypothesized mechanisms of PMM change. Recent work has found that the PMM is particularly sensitive to ITCZ shifts in intensity and location (Martinez-Villalobos and Vimont 2016). Other studies have suggested that the location of the ITCZ might inhibit or help types of Meridional Modes from occurring (Zhang et al. 2014a, b). In CESM-LME simulations, periods of high PMM activity

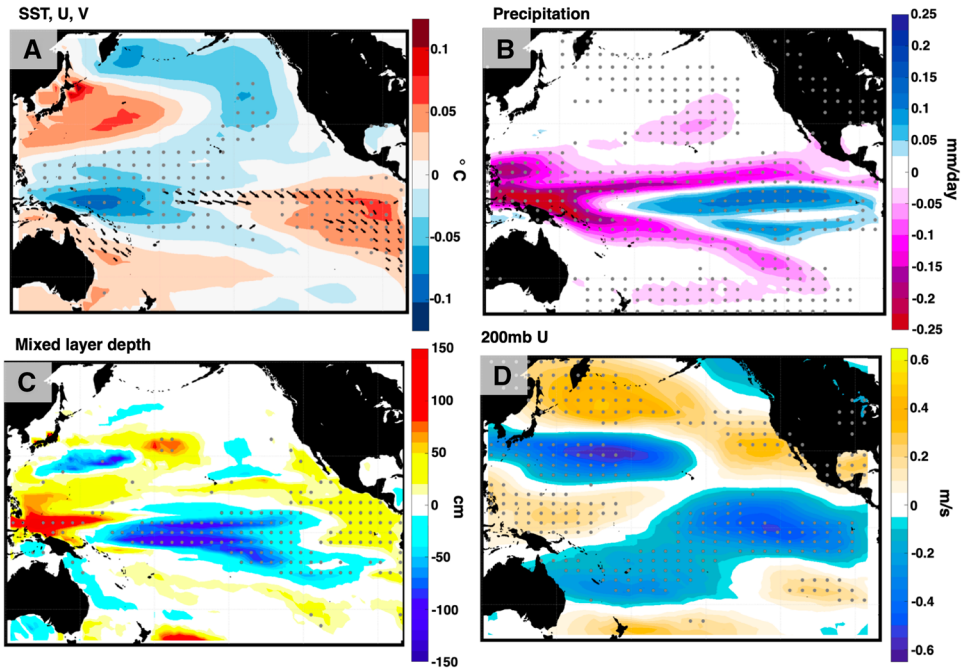

Fig. 4 Median least squares linear regression of DJF (+ 1) fields on the 30-year moving standard deviation of the PMM index from year 850 to 2006 in each of the 12 All-Forcing ensemble members. The median linear regression pattern between all 12 ensemble members encompasses 13,872 model years. Stippling indicates sign agreement in 100% of ensemble members. Similar patterns are also found when compositing the most extreme 20% of years (see Supplementary Materials.). Fields evaluated are **a** SST and surface wind anomalies, **b** Precipitation anomalies, **c** Mixed layer depth anomalies, and **d** 200 mb zonal wind anomalies

are indeed accompanied by a southward shifted ITCZ and a weaker Walker circulation; however, the magnitude of the meridional shift in ITCZ position in the model is small enough to preclude drawing conclusions of causality.

Similarly, we find minor variations in the sensitivity of latent heat flux in the western tropical North Pacific associated with the PMM variance (Fig. 5b). We calculate this sensitivity of latent heat flux to zonal winds, or Wind-Evaporation-SST Parameter, or "WES" parameter ($\propto$), using a linearized approximation as in Czaja et al. (2002) and Vimont et al. (2009).

$$-\propto(y)=\frac{\partial LH}{\partial u}=L_v C_e \rho\left(q_{sat}\left(T_s\right)-RHq_{sat}\left(T_{ref}\right)\right)\frac{u}{w}=LH\frac{u}{\bar{w}^2}$$

where LH is latent heat, u is zonal wind, $\bar{w}$ is wind speed ($\bar{w}=\sqrt{u^2+v^2+\hat{w}^2}$), $\hat{w}$ is a background wind speed used to account for higher frequency variance, $\hat{w}=4\ \mathrm{ms}^{-1}$ (Czaja et al. 2002), and $\propto$ has units of W s m^{-3} (annual mean field of $\propto$ illustrated in Fig. 5a). The WES parameter anomalies associated with the variance of the PMM are not only small in magnitude, but also occur in regions not particularly important for the activation of the PMM (Fig. 5b). In contrast, the change in latent heat flux sensitivity to the mean zonal winds expected under RCP8.5 forcing creates a far greater magnitude change; roughly a 20% increase in the mean WES feedback parameter is predicted in the RCP 8.5 extensions (Fig. 5c).

Finally, anomalies in atmospheric circulation can alter the characteristics of stochastic wind forcing in the extratropics, influencing the NPO and the PMM (Chiang et al. 2009). Using a simplified calculation for the strength of the jet stream (specifically, the 200 mb zonal wind averaged over wind speed between 20°N to 45°N and 110°E to 180°E in jet exit region over western Asia), a significant correlation is found between PMM activity and weakness of the jet stream, $R=-0.45$, $p<0.01$. Such an association is expected on general principles: when the jet stream is stronger (westerlies exceed 45 m/s), baroclinic eddy activity diminishes with reduced atmospheric noise (Nakamura 1992; Nakamura et al. 2002) thereby suppressing the NPO that ultimately forces the PMM (Chiang et al. 2009; Chiang and Fang 2010). This correlation is apparent in Fig. 4d: the slower the jet stream, the more energetic the variance of the PMM, and vice versa. As with the other hypothesized sources of PMM variability, however, the variations in 200 mb zonal wind speed found in the CESM-LME are so small, they cannot be prime drivers for PMM behavior.

Model magnitude aside, the ability of NPO variability to influence PMM variability merits greater investigation. In the LME, the ensemble mean correlation between the NPO (DJF) and following PMM (MAM) indices is $R=0.52$ at seasonal resolution in the All-Forcing Ensemble members, consistent with the expected causal relationship. Figure 6a, b, e, f further illustrates the mechanics of this relationship, showing the regions of significant ensemble mean correlation between December–January–February (DJF) wind anomalies and the concurrent NPO index (DJF) or the following PMM Index (March–April–May, MAM) using the 12 All-Forcing Ensemble Members of the CESM-LME with all 1156 years available. Figure 6a, e highlight the wind anomalies correlated with the NPO in DJF. Figure 6b, f illustrate the DJF wind anomalies correlated with a PMM event

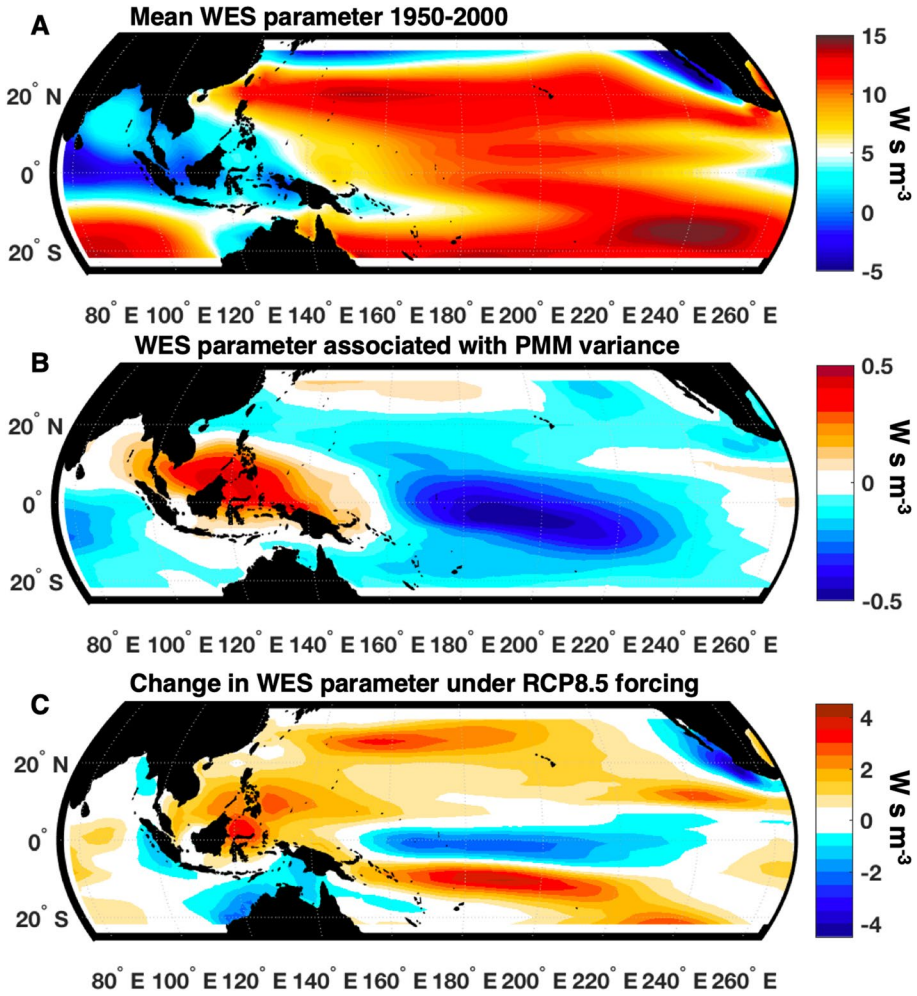

Fig. 5 Relationship between WES parameter and the Pacific Meridional Mode. **a** The annual mean field of WES feedback parameter (W s m^{-3}) over the 1950–2000 period, using the average of the 12 "All Forcing" ensemble members. In **b** the linear regression pattern associated with the natural variability of the Pacific Meridional Mode, methodology identical to climatological fields in Fig. 4. In **c** the difference between the 2080–2100 average under RCP 8.5 forcing and the present day mean (1950–2000) using the average of the four available RCP8.5 ensemble members (#2, 3, 8, 9)

following the subsequent MAM. The strong similarities in the pattern of anomalies confirm that the ideal conditions to initiate a PMM event are indeed supplied by the NPO. In the CESM-LME, the strong influence of the NPO on the PMM is centered in the central-western subtropical Pacific (10°–30°N, 165°–215°E), further westward than found in NCEP–NCAR Reanalysis version 1 (Kalnay et al. 1996), but in consistent spatial structures with reanalysis (Supplementary Fig. 3), and consistent with the model's PMM (as seen in Fig. 1b). The same is also true of the 30-year moving averages. Of particular importance is the high correlations in the trade wind region of the central equatorial Pacific (10°–30°N, 165°–215°E). As this is the same region where the NPO is known to influence the PMM, this suggests that the NPO may have a role in maintaining this PMM variance. There are, however, notable differences between the variance of the NPO and the variance of the PMM on wind variance (Fig. 6c, d, g, h); for example, the variance of the PMM is more highly correlated to equatorial Pacific wind variability, while the variance of the NPO is more highly correlated with the variance of higher latitude winds.

3.4 Mechanisms driving variance pattern

It is difficult to assess the fidelity of these model background climatic patterns associated with PMM variance in the instrumental record because observations are too short. Thus, we rely on the CESM models to take the broad approach of assessing whether the variance mode derives primarily from ocean or atmospheric dynamics. The CESM-LME control and two unforced control runs from the CESM Large Ensemble [CESM-LE, using a 1° latitude/longitude version of CAM5 (Kay et al. 2015)] are used to discriminate the role of the dynamical and thermodynamic mechanisms. In general, the CESM-LE was not created to model climate variability over the last millennium (Kay et al. 2015); instead, the project sought to create a multitude of ensemble members over the industrial era and future projections, including a fully coupled controlled experiment and a slab ocean experiment, used here. The variability of the PMM and the NPO are assessed in both the fully coupled CESM-LME Control (1155 years),

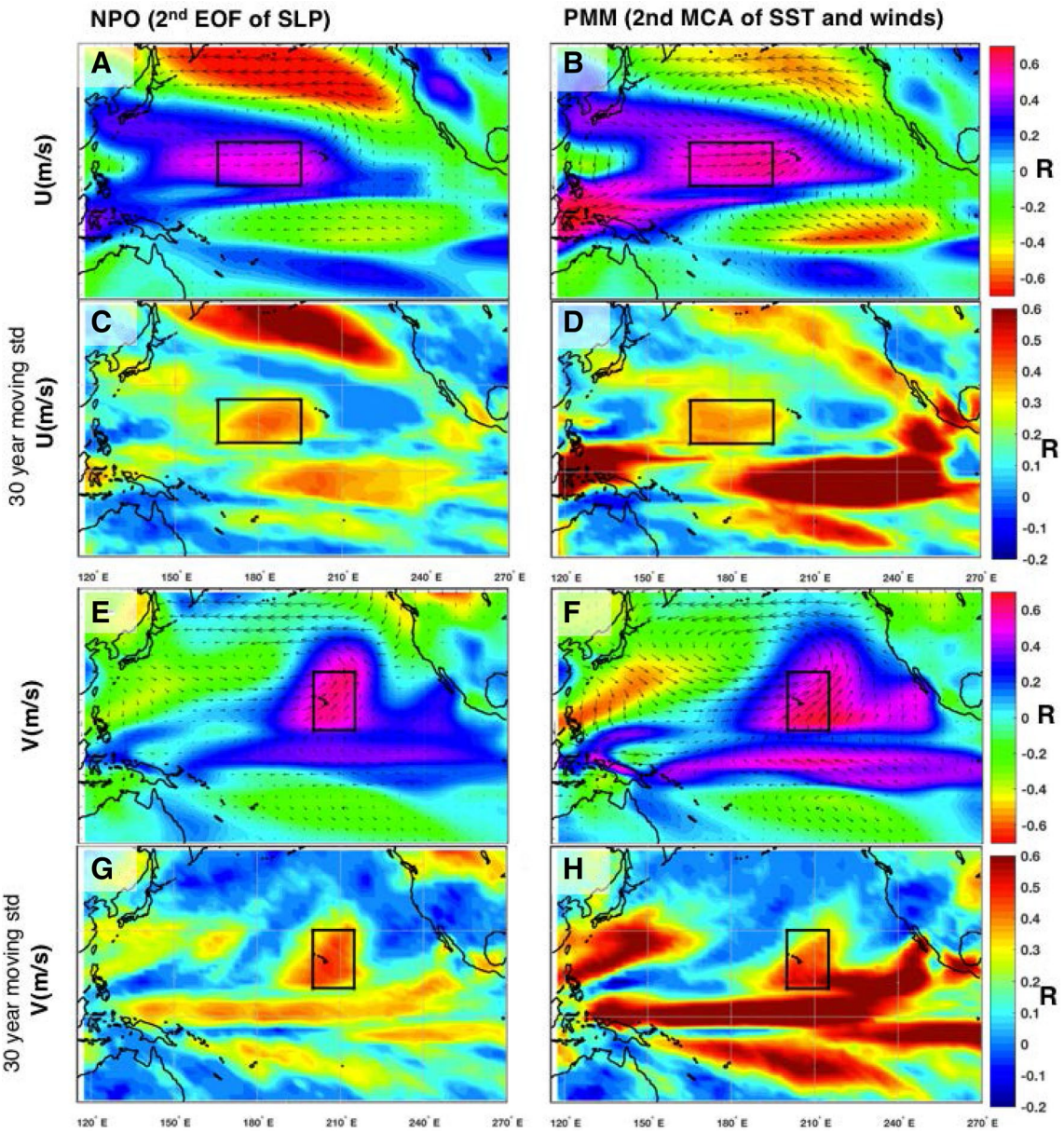

Fig. 6 Ensemble averaged DJF wind anomalies and variance associated with the North Pacific Oscillation (**a**, **c**, **e**, **g**) and Pacific Meridional Mode indices (**b**, **d**, **f**, **h**). **a** The Pearson correlation coefficient (R) of the DJF NPO index with the contemporaneous DJF zonal (U) winds averaged between all All-Forcing Ensemble members (N = 12 members, 1156 years per ensemble member, 13,872 years total). On top of this lies the linear regression coefficient of the NPO index with DJF U and V wind vectors for context. Bolded boxes represent the region where the NPO zonal winds are thought to influence the Pacific Meridional Mode in DJF in CESM-LME (10°–25°N, 165°–195°E). **b** Same as **a**, but for DJF zonal (U winds) and the following MAM PMM index. **c** The Pearson correlation coefficient of the 30-year moving standard deviation of the DJF NPO index with the 30-year moving standard deviation of the DJF zonal (U winds). **d** Same as **c**, but for the 30-year moving standard deviation of the PMM index. **e** Same as **a**, but for meridional (V) winds. The bolded box indicating the region where NPO meridional winds likely influence the Pacific Meridional Mode in DJF in CESM-LME (10°–30°N, 200°–215°E). **f** Same as **b**, but for meridional (V) winds. **g** Same as **c**, but for meridional (V) winds. **h** Same as **d**, but for meridional (V) winds

the fully coupled CESM-LE Control (1000 years), and the CESM-LE Slab Ocean Control (900 years).

In the slab ocean experiment the PMM is calculated using surface temperatures instead of SST; otherwise the treatment is identical to the previously described MCA method. There is consistency between the fully coupled and slab ocean experiments in the standard metrics of the PMM. For example, in the slab ocean experiment, the correlation of

the wind and SST expansion coefficient, or degree of air–sea connectivity, is 0.87, while both coupled model experiments observed values of 0.86 (observations R = 0.70). In each simulation, the PMM follows NPO variability and experiences maximum variance in MAM.

Multitaper mean spectrum analysis (Thomson 1982; Percival and Walden 1993; Ghil et al. 2002) suggests that both the LME and LE coupled ocean model experiments have statistically significant PMM variability in the 26–32 years bands at 95% significance (using 4 tapers, but still significant over a range of 2–8 tapers). However, there is no significant multidecadal variability observed in the slab ocean model (Fig. 7a), a result that emerges regardless of the number of tapers. This fundamental difference in behavior of the slab ocean model implies that the decadal frequencies observed in the PMM cannot be explained by an attenuation of stochastic white noise and ocean thermodynamics alone; some dynamical oceanic mechanism is required.

The region where NPO forcing is most influential on zonal winds is identified, (10°–25°N, 165°–195°E) and an index using the area averaged zonal wind components is created to assess any differences in the actual forcing of the PMM. We further find that there is no significant difference in the low frequency (> 10 years) component of the zonal wind forcing of the NPO (Fig. 7b). Neither the coupled model experiments nor the slab ocean model experiments exhibit statistically significant variability. Thus, the statistically significant decadal variability in the coupled models cannot be attributed to a low frequency component of atmospheric forcing. As the atmospheric forcing component in both the coupled and slab ocean models are similar, the significant decadal variability in the coupled models must result from some feedback process between the atmospheric forcing and ocean dynamics. These ocean dynamics are likely of equatorial origin; the relationship between PMM variance and mixed layer depth is most robust in the equatorial Pacific in the fully coupled experiments (Fig. 4c), and in the slab ocean experiment, the relationship between PMM variance and surface temperature differs most significantly from the fully coupled experiments in the equatorial Pacific (Supplementary Fig. 5). In the fully coupled experiments, periods of high PMM variance are accompanied by an anomalously cool North Pacific and western equatorial Pacific, while the eastern equatorial Pacific display mild warming. In the slab ocean experiment, periods of high PMM variance similarly occur with an anomalously cool North Pacific, but lack an association with the pronounced anomalous zonal dipole of equatorial surface temperature anomalies. Mechanisms for such oceanic feedbacks have been hypothesized, such as rectification of interannual variability onto thermocline stratification (Ogata et al. 2013; Rodgers et al. 2004).

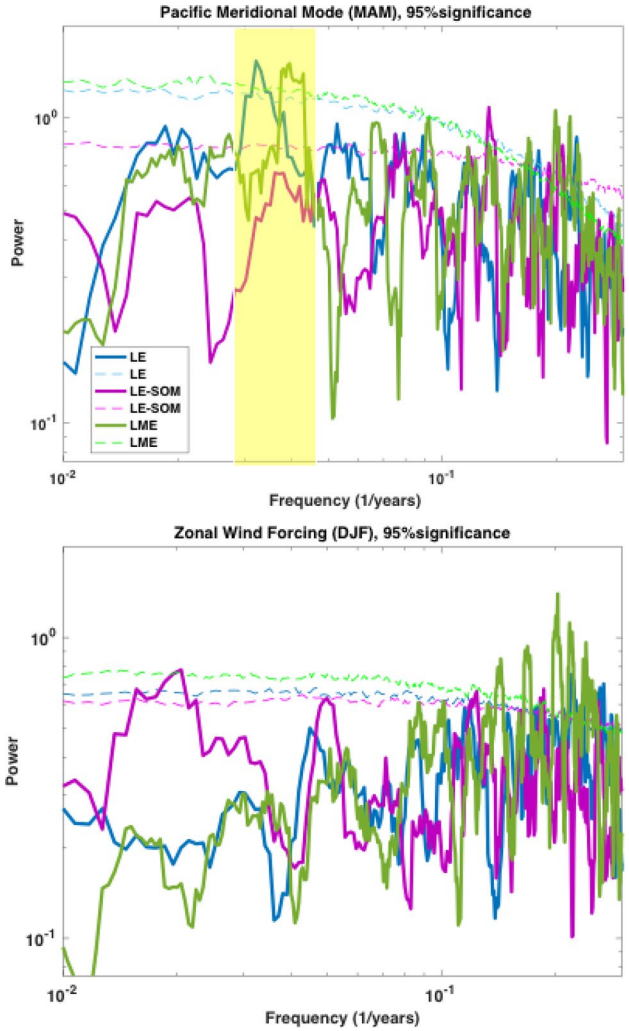

Fig. 7 Assessment of the necessity of ocean dynamics through contrasting experiments with and without an interactive ocean. We compare the (1) Control from the CESM-Last Millennium Ensemble (green, 1156 years), (2) control from the CESM Large Ensemble (to ensure that there are no critical differences when changing our spatial resolution between the LME and LE, blue, 1000 years) and 2). A slab ocean model with no ocean dynamics (pink, 900 years). We use multitaper spectral analysis (4 tapers) to assess the dominant frequencies in **a** the PMM index and **b** averaged zonal winds in the region most influential on the PMM (in CESM it is U averaged over 10°N to 25°N, 165° to 195°E, highlighted in green the box in Fig. 1b)

4 Summary and discussion

Modifications in the background climate have been hypothesized to alter the variability of the PMM. The CES-LME analysis shows some support for many of the most prominent hypothesized mechanisms, (ITCZ structure, sensitivity of latent heat flux to zonal winds, and North Pacific storminess,) but no single process mentioned here appears to dominate the unforced internal variation of the model PMM. Still,

a background climatological pattern associated with PMM variance emerges in the LME. This background state is characterized by cooler North Pacific sea surface temperatures, and weaker Walker circulation in the equatorial Pacific during periods of high PMM variance.

The spatial pattern of anomalies associated with high and low PMM variance are generally in agreement with previous studies that have noted the dynamical ink between the Western North Pacific and the NPO (Linkin and Nigam 2008; Baxter and Nigam 2015; Wang et al. 2012, 2014; Hartmann 2015): anomalous convection in the Western Tropical North Pacific (WTNP) generates atmospheric Rossby waves that can influence the NPO during the influential winter season (Wang et al. 2014; Furtado et al. 2012). The southern node of the NPO is thought to be highly influenced by atmospheric wave train activity from the equatorial Pacific (Furtado et al. 2012; Di Lorenzo et al. 2010). However, in CESM, this tropical atmospheric interaction cannot be the sole driving factor maintaining the statistically significant decadal variability in the PMM system. The atmospheric component of the slab ocean experiment is statistically indistinguishable from model runs with active ocean dynamics, yet the slab ocean simulations of the PMM do not feature significant decadal variability. Thus, the statistically significant variability at multidecadal timescales must require oceanic feedbacks. In the model, this oceanic feedback appears to be dominated by equatorial thermocline variability. Given the pattern and strength of correlations between PMM behavior and the equatorial Pacific found in the fully coupled experiments, ENSO dynamics are likely necessary to maintain this decadal variability. However, it is important to note that the pattern in the CESM mixed layer depth associated with PMM variance does not explicitly resemble the canonical ENSO response.

Thermocline variability has an important role in determining the interdecadal amplitude of ENSO (Ogata et al. 2013; Rodgers et al. 2004; Dewitte et al. 2007; Borlace et al. 2013). Periods of high ENSO variance have been associated with a deepening and sharpening of the thermocline (Ogata et al. 2013). A sharper thermocline increases the sensitivity of surface SST to thermocline displacement, which supports a positive feedback between ENSO and tropical Pacific decadal variability. Previous works have hypothesized mechanisms responsible for the low frequency modulation of ENSO (Li et al. 2013; Ogata et al. 2013; Chowdary et al. 2012; Rodgers et al. 2004; Meehl et al. 2001), many suggesting that ENSO variance is enhanced during periods of decreased zonal SST contrast, deeper eastern equatorial Pacific thermocline, and weaker Walker circulation (Meehl et al. 2001; Imada and Kimoto 2009; Kirtman and Schopf 1998; Kleeman et al. 1999; Barnett et al. 1999; Ogata et al. 2013; Sadekov et al. 2013). A feedback between ENSO amplitude modulation and the mean state of the equatorial Pacific has been described (Ogata et al. 2013, Imada and Kimoto 2009; Wittenberg 2009; Choi et al. 2012), however, it has been difficult to discern the causality of this relationship. The long integration model runs in this work provide evidence that, in the CESM-LME, the anomalous equatorial background pattern is the result of ENSO amplitude modulations, consistent with other work (Ogata et al. 2013; Rodgers et al. 2004; Liang et al. 2012; Sun and Zhang 2006). This work reaffirms that the PMM can initiate ENSO events (Fig. 2b) and that the variance of the PMM and ENSO are correlated (Fig. 2d). This work demonstrates that the background pattern of anomalies associated with PMM variance requires ENSO dynamics to operate (Fig. 7), and features robust anomalies in the equatorial Pacific mixed layer (Fig. 4c). Furthermore, this work highlights that the amplitude modulations are, in part, influenced by the North Pacific atmosphere (Fig. 6). Complementary to the work presented here, Okumura et al. (2017) found that both ENSO and extratropical variability are important in setting prominent Pacific decadal variability in CCSM4. It is interesting that the pattern associated with the interdecadal amplitude modulation of ENSO in CCSM4 strongly resembles the cooler North Pacific/weaker-Walker zonal pattern in the equatorial Pacific associated with the PMM variance pattern described here.

These results support prior studies showing distinct, yet necessary roles for subtropical atmospheric noise and equatorial dynamics in maintaining decadal variability (Di Lorenzo et al. 2015; Okumura et al. 2017). Di Lorenzo et al. (2015) divided the influence of "meridional" and "zonal" modes on decadal variability, noting that the PMM can supply decadal and multidecadal variability to the tropics, while ENSO dynamics amplify that variability through global teleconnections. Okumura et al. (2017) further illustrated that influences from other regions, particularly the South Pacific, may have an important role in mediating Pacific variability.

An outstanding question is if the PMM's ability to influence decadal variability and ENSO has varied throughout time. While the instrumental record is too short to directly compare observations with the model-based results, there is observational evidence that central Pacific El Niño events, dynamically linked to the PMM, become more prevalent during colder North Pacific conditions (Xiang et al. 2013; McPhaden et al. 2011; Chung and Li 2013; Choi et al. 2012).

During a period known as the Little Ice Age (LIA), spanning years 1400–1850, paleoclimate proxies provide evidence for persistent climate anomalies, most notably cooler Northern Hemispheric surface temperatures ~ 0.6 to 0.8 °C (Mann et al. 1998, 2009), despite smaller anomalies in mean global temperature (IPCC AR4) (Change 2007). Physically constrained general circulation models have a difficult time reproducing the magnitude of the anomalies expressed in paleoclimate proxies during the LIA. This may be partially

the result of inaccuracies in model physics, and partially due to the interpretation of limited samples of the paleoproxy record. As such, we cannot assess the response of the PMM to mean state changes during the LIA in the CESM-LME. Nevertheless, we can describe some of the expected sense of change in the PMM associated with the mean state. In the LME, heightened PMM activity is associated with mean state anomalies featuring cooler North Pacific surface temperatures, weakened Walker circulation, El-Niño-like equatorial surface temperatures, an equatorially displaced ITCZ and heightened ENSO activity. Paleoclimate proxies demonstrate that the LIA featured pronounced northern hemisphere cooling (Mann et al. 1998), equatorward displacement of ITCZ (Sachs et al. 2009), or an ITCZ significantly different in structure (Denniston et al. 2016; Lechleitner et al. 2017). In several reconstructions, ENSO variance increases throughout the LIA, reaching a maximum over the sixteenth to nineteenth century (Li et al. 2013; Rustic et al. 2015; Loisel et al. 2017). Palmyra corals also record especially intense ENSO activity over the seventeenth century (Cobb et al. 2003). Studies have suggested that this change in ENSO activity was accompanied by a modification in the mean equatorial zonal gradient, from a strong zonal gradient in the early LIA to a weaker zonal gradient over the sixteenth to nineteenth century (Rustic et al. 2015). Additionally, proxies in regions associated with PMM influence, such as continental North America, or higher latitude North Pacific also show heightened decadal variability during the early nineteenth century (Sanchez et al. 2016; Halfar et al. 2011; Hetzinger et al. 2012; MacDonald and Case 2005; Griffin and Anchukaitis 2014). Thus, while they are scattered, these paleo observations are generally consistent with the sense, if not the magnitude of the model results. However, our analysis also highlights the fact that the reconstruction of thermocline variability in the equatorial Pacific over the last millennium would be a particularly important target for further exploration of PMM activity in paleo archives.

What does the CESM-LME behavior imply for the future behavior of the PMM? Unforced, internal variability alone can modulate the moving standard deviation of the PMM by a factor of two in the model. In single ensemble members, this internal variability dominates, while forced changes, such as volcanic eruptions, can influence the PMM, but the link between this radiative cooling effect and PMM behavior is not robust (Supplementary Materials Figure S4). On the other hand, simulations that extend the "All Forcing" experiments with RCP8.5 greenhouse gas forcing continued out through year 2100 result in PMM variance that exceed the bounds of that simulated over last millennium (Fig. 3c). PMM variance at the "present" (2006) is not unusual with respect to the last millennium, but the RCP 8.5 extensions of the "All Forcing" experiments exhibit a 33% increase in standard deviation of the PMM relative to the 2006 average by year 2100. This result is similar to that of Liguori and Di Lorenzo (2018). Some notable differences in the RCP8.5 scenario accompany this increase in variance. For example, the mean WES feedback parameter increases in the trade wind region, implying a heightened sensitivity of latent heat flux to zonal winds (Fig. 5c).

This result underscores the fact that anthropogenically forced change in PMM variability is quite distinct from the unforced, internal modulation described in depth here. In this regard, the model differences between forced and unforced PMM activity could be useful for attribution of the steady increase in variance of the PMM over the late twentieth century and early twenty-first century. For example, the lack of clear instrumental evidence for a trend in the WES feedback parameter over this same period may suggest that the increasing variance of the PMM is not (yet) the direct result of anthropogenic forcing—an issue worthy of further work (Liguori and Di Lorenzo 2018). In any case, the model clearly demonstrates that the PMM is capable of high amplitude shifts in variance, unprompted by any modifications in radiative forcing, and that these that can have a profound influence on the state of the tropical Pacific.

Acknowledgements The authors would like to thank two anonymous reviewers and the editor for their constructive comments. The authors would also like to acknowledge CESM1 (CAM5) Last Millennium Ensemble Community Project and supercomputing resources provided by NSF/CISL/Yellowstone. Salary support for SCS was provided by NSF14-59726, to CDC. AJM and DJA were partially supported by NSF (OCE1419306) and NOAA (MAPP, NA17OAR4310106). Support for DJA additionally came from the NSF Graduate Research Fellowship (DGE-1144086).

References

Amaya DJ, DeFlorio MJ, Miller AJ, Xie SP (2017) WES feedback and the Atlantic Meridional Mode: observations and CMIP5 comparisons. Clim Dyn 49(5–6):1665–1679

Anderson BT (2003) Tropical Pacific sea surface temperatures and preceding sea level pressure anomalies in the subtropical North Pacific. J Geophys Res 108:4732. https://doi.org/10.1029/2003JD003805

Barnett TP, Pierce DW, Latif M, Dommenget D, Saravanan R (1999) Interdecadal interactions between the tropics and midlatitudes in the Pacific basin. Geophys Res Lett 26(5):615–618

Baxter S, Nigam S (2015) Key role of the North Pacific Oscillation–west Pacific pattern in generating the extreme 2013/14 North American winter. J Clim 28(20):8109–8117

Borlace S, Cai W, Santoso A (2013) Multidecadal ENSO amplitude variability in a 1000-yr simulation of a coupled global climate model: implications for observed ENSO variability. J Clim 26(23):9399–9407

Bretherton CS, Widmann M, Dymnikov VP, Wallace JM, Bladé I (1999) The effective number of spatial degrees of freedom of a time-varying field. J Clim 12(7):1990–2009

Capotondi A, Wittenberg A, Masina S (2006) Spatial and temporal structure of tropical Pacific interannual variability in 20th century coupled simulations. Ocean Model 15(3–4):274–298

Chang P, Ji L, Li H (1997) A decadal climate variation in the tropical Atlantic Ocean from thermodynamic air–sea interactions. Nature 385(6616):516

Chang P, Zhang L, Saravanan R, Vimont DJ, Chiang JC, Ji L, Seidel H, Tippett MK (2007) Pacific meridional mode and El Niño–Southern oscillation. Geophys Res Lett 34:L16608. https://doi.org/10.1029/2007GL030302

Change IC (2007) The fourth assessment report of the intergovernmental panel on climate change. Cambridge University Press, Geneva

Chiang JC, Fang Y (2010) Was the North Pacific wintertime climate less stormy during the mid-Holocene? J Clim 23(14):4025–4037

Chiang JC, Vimont DJ (2004) Analogous Pacific and Atlantic meridional modes of tropical atmosphere–ocean variability. J Clim 17(21):4143–4158

Chiang JCH, Fang Y, Chang P (2009) Pacific climate change and ENSO activity in the mid-Holocene. J Clim 22(4):923–939

Choi J, An SI, Yeh SW (2012) Decadal amplitude modulation of two types of ENSO and its relationship with the mean state. Clim Dyn 38(11–12):2631–2644

Chowdary JS, Xie SP, Tokinaga H, Okumura YM, Kubota H, Johnson N, Zheng XT (2012) Interdecadal variations in ENSO teleconnection to the Indo–western Pacific for 1870–2007. J Clim 25(5):1722–1744

Chung PH, Li T (2013) Interdecadal relationship between the mean state and El Niño types. J Clim 26(2):361–379

Cobb KM, Charles CD, Cheng H, Edwards RL (2003) El Niño/Southern Oscillation and tropical Pacific climate during the last millennium. Nature 424(6946): 271

Czaja A, Van der Vaart P, Marshall J (2002) A diagnostic study of the role of remote forcing in tropical Atlantic variability. J Clim 15(22):3280–3290

Denniston RF, Ummenhofer CC, Wanamaker AD, Lachniet MS, Villarini G, Asmerom Y, Polyak VJ, Passaro KJ, Cugley J, Woods D, Humphreys WF (2016) Expansion and contraction of the Indo-Pacific tropical rain belt over the last three millennia. Sci Rep 6:34485

Deser C, Phillips AS, Tomas RA, Okumura YM, Alexander MA, Capotondi A, Scott JD, Kwon YO, Ohba M (2012a) ENSO and Pacific decadal variability in the Community Climate System Model version 4. J Clim 25(8):2622–2651

Deser C, Phillips A, Bourdette V, Teng H (2012b) Uncertainty in climate change projections: the role of internal variability. Clim Dyn 38(3–4):527–546

Dewitte B, Yeh SW, Moon BK, Cibot C, Terray L (2007) Rectification of ENSO variability by interdecadal changes in the equatorial background mean state in a CGCM simulation. J Clim 20(10):2002–2021

Di Lorenzo E, Mantua N (2016) Multi-year persistence of the 2014/15 North Pacific marine heatwave. Nat Clim Change 6:1042

Di Lorenzo E, Cobb KM, Furtado JC, Schneider N, Anderson BT, Bracco A, Alexander MA, Vimont DJ (2010) Central Pacific El Niño and decadal climate change in the North Pacific Ocean. Nat Geosci 3(11):762–765

Di Lorenzo E, Liguori G, Schneider N, Furtado JC, Anderson BT, Alexander MA (2015) ENSO and meridional modes: a null hypothesis for Pacific climate variability. Geophys Res Lett 42(21):9440–9448

Furtado JC, Di Lorenzo E, Anderson BT, Schneider N (2012) Linkages between the North Pacific Oscillation and central tropical Pacific SSTs at low frequencies. Clim Dyn 39(12):2833–2846

Ghil M, Allen MR, Dettinger MD, Ide K, Kondrashov D, Mann ME, Robertson AW, Saunders A, Tian Y, Varadi F, Yiou P (2002) Advanced spectral methods for climatic time series. Rev Geophys 40(1):3

Griffin D, Anchukaitis KJ (2014) How unusual is the 2012–2014 California drought? Geophys Res Lett 41(24):9017–9023

Guillet S, Corona C, Stoffel M, Khodri M, Lavigne F, Ortega P, Eckert N, Sielenou PD, Daux V, Churakova OV, Davi N (2017) Climate response to the Samalas volcanic eruption in 1257 revealed by proxy records. Nat Geosci 10(2):123

Halfar J, Williams B, Hetzinger S, Steneck RS, Lebednik P, Winsborough C, Omar A, Chan P, Wanamaker AD Jr (2011) 225 years of Bering Sea climate and ecosystem dynamics revealed by coralline algal growth-increment widths. Geology 39(6):579–582

Ham YG, Kug JS (2012) How well do current climate models simulate two types of El Nino? Clim Dyn 39(1–2):383–398

Hartmann DL (2015) Pacific sea surface temperature and the winter of 2014. Geophys Res Lett 42(6):1894–1902

Hetzinger S, Halfar J, Mecking JV, Keenlyside NS, Kronz A, Steneck RS, Adey WH, Lebednik PA (2012) Marine proxy evidence linking decadal North Pacific and Atlantic climate. Clim Dyn 39(6):1447–1455

Imada Y, Kimoto M (2009) ENSO amplitude modulation related to Pacific decadal variability. Geophys Res Lett 36:L03706. https://doi.org/10.1029/2008GL036421

Joh Y, Di Lorenzo E (2017) Increasing coupling between NPGO and PDO leads to prolonged marine heatwaves in the Northeast Pacific. Geophys Res Lett 44(22)

Kalnay E, Kanamitsu M, Kistler R, Collins W, Deaven D, Gandin L, Iredell M, Saha S, White G, Woollen J, Zhu Y (1996) The NCEP/NCAR 40-year reanalysis project. Bull Am Meteorol Soc 77(3):437–471

Kay JE, Deser C, Phillips A, Mai A, Hannay C, Strand G, Arblaster JM, Bates SC, Danabasoglu G, Edwards J, Holland M (2015) The Community Earth System Model (CESM) large ensemble project: a community resource for studying climate change in the presence of internal climate variability. Bull Am Meteorol Soc 96(8):1333–1349

Kim ST, Yu JY (2012) The two types of ENSO in CMIP5 models. Geophys Res Lett 39:L11704. https://doi.org/10.1029/2012GL052006

Kirtman BP, Schopf PS (1998) Decadal variability in ENSO predictability and prediction. J Clim 11(11):2804–2822

Kleeman R, McCreary JP, Klinger BA (1999) A mechanism for generating ENSO decadal variability. Geophys Res Lett 26(12):1743–1746

Kug JS, Choi J, An SI, Jin FF, Wittenberg AT (2010) Warm pool and cold tongue El Niño events as simulated by the GFDL 2.1 coupled GCM. J Clim 23(5):1226–1239

Larson S, Kirtman B (2013) The Pacific Meridional Mode as a trigger for ENSO in a high-resolution coupled model. Geophys Res Lett 40(12):3189–3194

Lavigne F, Degeai JP, Komorowski JC, Guillet S, Robert V, Lahitte P, Oppenheimer C, Stoffel M, Vidal CM, Pratomo I, Wassmer P (2013) Source of the great AD 1257 mystery eruption unveiled, Samalas volcano, Rinjani Volcanic Complex, Indonesia. Proc Natl Acad Sci 110(42):16742–16747

Lechleitner FA, Breitenbach SF, Rehfeld K, Ridley HE, Asmerom Y, Prufer KM, Marwan N, Goswami B, Kennett DJ, Aquino VV, Polyak V (2017) Tropical rainfall over the last two millennia: evidence for a low-latitude hydrologic seesaw. Sci Rep 7:45809

Li J, Xie SP, Cook ER, Morales MS, Christie DA, Johnson NC, Chen F, D'Arrigo R, Fowler AM, Gou X, Fang K (2013) El Niño modulations over the past seven centuries. Nat Clim Change 3(9):822

Liang J, Yang XQ, Sun DZ (2012) The effect of ENSO events on the tropical Pacific mean climate: Insights from an analytical model. J Clim 25(21):7590–7606

Liguori G, Di Lorenzo E (2018) Meridional modes and increasing Pacific decadal variability under anthropogenic forcing. Geophys Res Lett 45:983–991

Lin CY, Yu JY, Hsu HH (2015) CMIP5 model simulations of the Pacific meridional mode and its connection to the two types of ENSO. Int J Climatol 35(9):2352–2358

Linkin ME, Nigam S (2008) The North Pacific Oscillation–west Pacific teleconnection pattern: mature-phase structure and winter impacts. J Clim 21(9):1979–1997

Loisel J, MacDonald GM, Thomson MJ (2017) Little Ice Age climatic erraticism as an analogue for future enhanced hydroclimatic variability across the American Southwest. PLoS One 12(10):e0186282

MacDonald GM, Case RA (2005) Variations in the Pacific Decadal oscillation over the past millennium. Geophys Res Lett 32:L08703. https://doi.org/10.1029/2005GL022478

Mann ME, Bradley RS, Hughes MK (1998) Global-scale temperature patterns and climate forcing over the past six centuries. Nature 392(6678):779

Mann ME, Zhang Z, Rutherford S, Bradley RS, Hughes MK, Shindell D, Ammann C, Faluvegi G, Ni F (2009) Global signatures and dynamical origins of the Little Ice Age and Medieval Climate Anomaly. Science 326(5957):1256–1260

Martinez-Villalobos C, Vimont DJ (2016) The role of the mean state in Meridional mode structure and growth. J Clim 29(10):3907–3921

McPhaden MJ, Lee T, McClurg D (2011) El Niño and its relationship to changing background conditions in the tropical Pacific Ocean. Geophys Res Lett 38:L15709. https://doi.org/10.1029/2011GL048275

Meehl GA, Gent PR, Arblaster JM, Otto-Bliesner BL, Brady EC, Craig A (2001) Factors that affect the amplitude of El Niño in global coupled climate models. Clim Dyn 17(7):515–526

Nakamura H (1992) Midwinter suppression of baroclinic wave activity in the Pacific. J Atmos Sci 49(17):1629–1642

Nakamura H, Izumi T, Sampe T (2002) Interannual and decadal modulations recently observed in the Pacific storm track activity and East Asian winter monsoon. J Climate 15:1855–1874

Ogata T, Xie SP, Wittenberg A, Sun DZ (2013) Interdecadal amplitude modulation of El Niño-Southern Oscillation and its impact on tropical Pacific decadal variability. J Clim 26(18):7280–7297

Okumura YM, Sun T, Wu X (2017) Asymmetric modulation of El Niño and La Niña and the linkage to tropical Pacific decadal variability. J Clim 30(12):4705–4733

Otto-Bliesner BL, Brady EC, Fasullo J, Jahn A, Landrum L, Stevenson S, Rosenbloom N, Mai A, Strand G (2016) Climate variability and change since 850 CE: an ensemble approach with the community earth system model. Bull Am Meteorol Soc 97(5):735–754

Percival DB, Walden AT (1993) Spectral analysis for physical applications, vol 583. Cambridge University Press, New York

Rodgers KB, Friederichs P, Latif M (2004) Tropical Pacific decadal variability and its relation to decadal modulations of ENSO. J Clim 17(19):3761–3774

Rogers JC (1981) The north Pacific oscillation. Int J Climatol 1(1):39–57

Rustic GT, Koutavas A, Marchitto TM, Linsley BK (2015) Dynamical excitation of the tropical Pacific Ocean and ENSO variability by Little Ice Age cooling. Science 350:1537–1541

Sachs JP, Sachse D, Smittenberg RH, Zhang Z, Battisti DS, Golubic S (2009) Southward movement of the Pacific intertropical convergence zone AD 1400–1850. Nat Geosci 2(7):519–525

Sadekov AY, Ganeshram R, Pichevin L, Berdin R, McClymont E, Elderfield H, Tudhope AW (2013) Palaeoclimate reconstructions reveal a strong link between El Niño–Southern Oscillation and Tropical Pacific mean state. Nat Commun 4:2692

Sanchez SC, Charles CD, Carriquiry JD, Villaescusa JA (2016) Two centuries of coherent decadal climate variability across the Pacific North American region. Geophys Res Lett 43(17):9208–9216

Smith TM, Reynolds RW, Peterson TC, Lawrimore J (2008) Improvements to NOAA's historical merged land–ocean surface temperature analysis (1880–2006). J Clim 21(10):2283–2296

Sun D-Z, Zhang T (2006) A regulatory effect of ENSO on the time-mean thermal stratification of the equatorial upper ocean. Geophys Res Lett 33:L07710. https://doi.org/10.1029/2005GL025296

Thomson DJ (1982) Spectrum estimation and harmonic analysis. Proc IEEE 70:1055–1096

Vega-Westhoff B, Sriver RL (2017) Analysis of ENSO's response to unforced variability and anthropogenic forcing using CESM. Sci Rep 7(1):18047

Vimont DJ (2005) The contribution of the interannual ENSO cycle to the spatial pattern of decadal ENSO-like variability. J Clim 18(12):2080–2092

Vimont DJ, Wallace JM, Battisti DS (2003) The seasonal footprinting mechanism in the Pacific: implications for ENSO. J Clim 16(16):2668–2675

Vimont DJ, Alexander M, Fontaine A (2009) Midlatitude excitation of tropical variability in the Pacific: the role of thermodynamic coupling and seasonality. J Clim 22(3):518–534

Vimont DJ, Alexander MA, Newman M (2014) Optimal growth of central and east Pacific ENSO events. Geophys Res Lett 41(11):4027–4034

Walker GT, Bliss EW (1932) World weather. V Mem R Meteorol Soc 4:53–84

Wang SY, L'Heureux M, Chia HH (2012) ENSO prediction one year in advance using western North Pacific sea surface temperatures. Geophys Res Lett 39:L05702. https://doi.org/10.1029/2012GL050909

Wang SY, Hipps L, Gillies RR, Yoon JH (2014) Probable causes of the abnormal ridge accompanying the 2013–2014 California drought: ENSO precursor and anthropogenic warming footprint. Geophys Res Lett 41(9):3220–3226

Wittenberg AT (2009) Are historical records sufficient to constrain ENSO simulations? Geophys. Res Lett 36:L12702. https://doi.org/10.1029/2009GL038710

Xiang B, Wang B, Li T (2013) A new paradigm for the predominance of standing central Pacific warming after the late 1990s. Clim Dyn 41(2):327–340

Xie SP, Philander SGH (1994) A coupled ocean-atmosphere model of relevance to the ITCZ in the eastern Pacific. Tellus A 46(4):340–350

Yu JY, Kim ST (2011) Relationships between extratropical sea level pressure variations and the central Pacific and eastern Pacific types of ENSO. J Clim 24(3):708–720

Yu JY, Kao HY, Lee T (2010) Subtropics-related interannual sea surface temperature variability in the central equatorial Pacific. J Clim 23(11):2869–2884

Zhang L, Chang P, Ji L (2009) Linking the Pacific meridional mode to ENSO: coupled model analysis. J Clim 22(12):3488–3505

Zhang H, Clement A, Di Nezio P (2014a) The South Pacific meridional mode: a mechanism for ENSO-like variability. J Clim 27(2):769–783

Zhang H, Deser C, Clement A, Tomas R (2014b) Equatorial signatures of the Pacific Meridional Modes: dependence on mean climate state. Geophys Res Lett 41(2):568–574

Zhang W, Vecchi GA, Murakami H, Villarini G, Jia L (2016) The Pacific meridional mode and the occurrence of tropical cyclones in the western North Pacific. J Clim 29(1):381–398